Dynamic Nuclear Polarization by Electrical Spin Injection in Ferromagnet-Semiconductor Heterostructures

J. Strand,[1] B. D. Schultz,[2] A. F. Isakovic,[1] C. J. Palmstrøm,[2] and P. A. Crowell[1,*]

[1]*School of Physics and Astronomy, University of Minnesota, Minneapolis, Minnesota 55455, USA*

[2]*Department of Chemical Engineering and Materials Science, University of Minnesota, Minneapolis, Minnesota 55455, USA*

(Received 19 February 2003; published 18 July 2003)

Electrical spin injection from Fe into $Al_xGa_{1-x}As$ quantum well heterostructures is demonstrated in small (< 500 Oe) in-plane magnetic fields. The measurement is sensitive only to the component of the spin that precesses about the internal magnetic field in the semiconductor. This field is much larger than the applied field and depends strongly on the injection current density. Details of the observed hysteresis in the spin injection signal are reproduced in a model that incorporates the magnetocrystalline anisotropy of the epitaxial Fe film, spin relaxation in the semiconductor, and the dynamic polarization of nuclei by the injected spins.

DOI: 10.1103/PhysRevLett.91.036602 PACS numbers: 72.25.Hg, 72.25.Rb, 76.60.Jx

The injection of spin from a conventional ferromagnetic metal into a semiconductor is a prerequisite for several proposed magnetoelectronic devices [1]. Although spin transport across the ferromagnet-semiconductor (FM-S) interface has recently been demonstrated [2–5], most injection experiments on metallic FM-S systems have used GaAs quantum wells as optical spin detectors. These experiments are sensitive only to the component of the spin perpendicular to the interface between the ferromagnet and the semiconductor. Saturating the magnetization in the perpendicular direction requires magnetic fields in excess of several kilogauss due to the shape anisotropy of the film. In contrast, the most useful properties of typical ferromagnetic thin films, such as low-field switching and hysteresis, can be exploited only by coupling to the *in-plane* component of the magnetization [6]. In the case of metallic FM-S structures, in-plane coupling has been observed only as a small change in transport properties [2] or using optically pumped carriers [7,8].

In this Letter we report a demonstration of electrical spin injection in FM-S heterostructures using small (< 500 Oe) in-plane magnetic fields. We measure only the component of the spin that precesses after injection into the semiconductor using electroluminescence polarization (ELP) as a detection technique [6,9]. The effective magnetic field inducing the precession depends strongly on the electrical bias conditions and is dramatically enhanced at the highest injection current densities. The origin of the hysteresis in the spin polarization signal is magnetization reversal in the ferromagnet, but the magnitude and shape of the observed loops depend on the effective field in the semiconductor. Modeling based on the results of optical pumping experiments demonstrates that the origin of the large effective field is dynamic nuclear polarization due to the spin-polarized current injected from the ferromagnet [10–12]. This approach to dynamic nuclear polarization in semiconductors is a simple alternative to the use of optical pumping or high magnetic fields as sources of spin-polarized electrons [13,14].

We report results from two heterostructures with different quantum well (QW) spin detectors. The samples are grown by molecular beam epitaxy on p^+ GaAs (100) substrates and consist of p-$Al_xGa_{1-x}As$/QW/n-$Al_xGa_{1-x}As$/Fe/Al. Intrinsic setback layers are placed on both sides of the QW, and the resulting p-i-n structure forms a light-emitting diode (LED). The 50 Å thick iron and the 25 Å Al layers are grown *in situ* at $\approx 0\,^{\circ}$C. A Si δ-doped layer ($\delta = 2 \times 10^{13}$ atoms/cm^2 for sample A and 3×10^{13} atoms/cm^2 for sample B) is grown 25 Å below the Fe-semiconductor interface in order to form a tunneling contact. For sample A, $x = 0.2$ and the QW is 100 Å $Al_{0.1}Ga_{0.9}As$ with p-doped barriers. For sample B, $x = 0.1$ and the QW is 100 Å GaAs with intrinsic barriers. The important difference between the samples is the effective g factor g^* for electrons in the QW. For sample B, $g^* \approx -0.4$, while sample A was designed to have a g factor close to zero [15]. The magnetocrystalline anisotropy of the epitaxial Fe film results in easy and hard axes along [011] and [01$\bar{1}$], as shown in Fig. 1.

The samples are processed into 200 μm wide mesas. The ferromagnetic contact is 80 μm wide, and a 40 μm wide gold contact is evaporated over the center of the bar, which is cleaved into pieces 1–1.5 mm long. A schematic cross section is shown in Fig. 1. The devices are operated with the Schottky contact under reverse bias and the p-i-n LED under forward bias. Electrons tunnel from the Fe into the n layer and recombine in the QW with holes supplied by the substrate. Electroluminescence (EL) is observed for current densities above ≈ 1 A/cm^2, with leakage causing some variation in the threshold current from sample to sample. The EL, which is dominated by heavy-hole recombination, is collected along the sample normal $\hat{\mathbf{z}}$ from the exposed semiconductor mesa and through the semitransparent ferromagnetic film. The

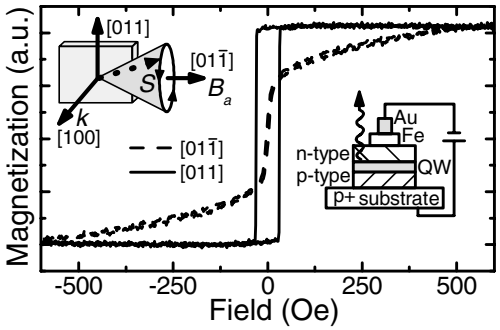

FIG. 1. In-plane magnetization of the epitaxial Fe film (sample A) parallel to fields applied along [011] and [01$\bar{1}$]. Left inset: schematic of the experimental setup. The direction of light propagation $\hat{\mathbf{k}}$ is along the sample normal, $\mathbf{B}_a$ is the applied field, and $\mathbf{S}$ is the precessing spin in the semiconductor. Right inset: cross-sectional schematic of the device.

circular polarization of the EL, which we refer to as the ELP signal, is equal to the electron spin polarization along $\hat{\mathbf{z}}$ at the time of recombination.

Although spin injection can be observed in these devices when a magnetic field is applied along the sample normal $\hat{\mathbf{z}}$ [3–5], we focus here on the transverse field configuration, $\hat{\mathbf{k}} \parallel \hat{\mathbf{z}} \perp \mathbf{B}_a$, where $\hat{\mathbf{k}}$ is the direction of light propagation, and $\mathbf{B}_a$ is the magnetic field applied in the plane of the sample, as shown in the left inset of Fig. 1. In this geometry the magnetocrystalline anisotropy of the Fe film allows for a significant angle between the electron spin $\mathbf{S}$ and $\mathbf{B}_a$. The magnetization remains in the sample plane and $\mathbf{S}$ precesses out of the plane after injection into the semiconductor. This approach is related philosophically to the oblique Hanle effect [11], in which optically pumped spins are created at an angle $0 < \theta < \pi/2$ with respect to the applied field, an approach followed in the recent electrical spin injection experiment of Motsnyi *et al.* [5]. An important advantage of our approach is that we detect only the precessing component of the spin, making the measurement essentially immune to background effects.

Figures 2(a) and 2(b) show the ELP signal as a function of the transverse magnetic field, which is applied in the sample plane at a small angle ($4° \pm 2°$) from the [01$\bar{1}$] axis. Data are shown at several different current densities for samples A and B. At the lowest current densities, just above the threshold for light emission, the ELP signal is nearly independent of the applied magnetic field and shows no hysteresis, although there is a polarization offset of 0%–2.5%. As the current density is increased, a double loop structure develops. In the case of sample A [Fig. 2(a)], the magnitude of the polarization signal increases with increasing bias, reaching a maximum value of approximately 4%, determined from the peak-to-peak height of the loop. In the case of sample B [Fig. 2(b)], both the magnitude *and the shape* of the observed loops depend on the current density. A maximum in the signal is observed at a current density of approximately 3.5 A/cm^2, above which the signal decreases and the central dip in the loop becomes much narrower. Photoluminescence (PL) measurements on the same structures with a linearly polarized pump show no polarization signal in a transverse magnetic field.

The origin of the ELP signal observed in Fig. 2 is a precession of the spin injected from the ferromagnet. The observed polarization depends on the angle between $\mathbf{B}_a$ and the magnetization $\mathbf{M}$ of the Fe film as well as the precession frequency and spin relaxation time in the QW.

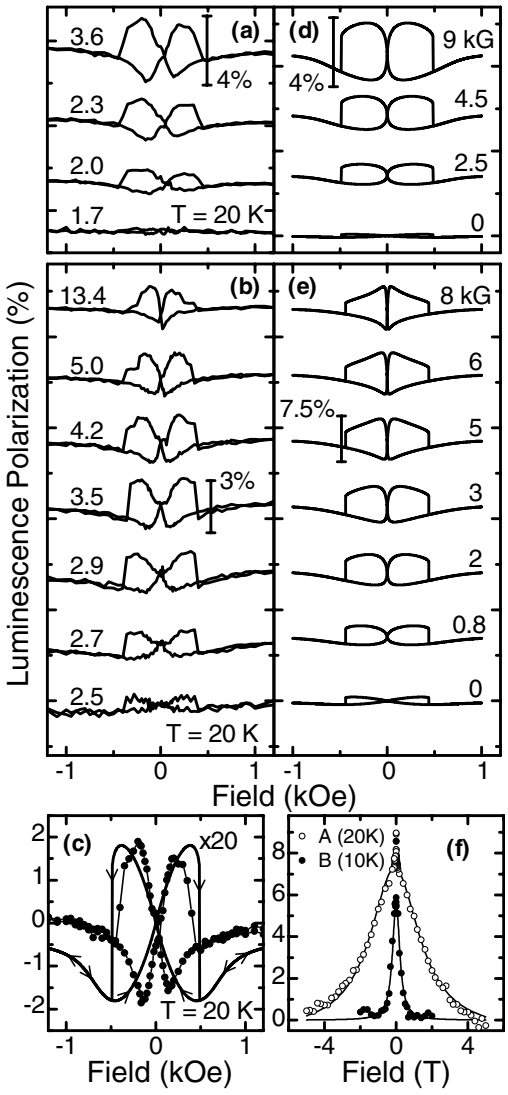

FIG. 2. (a),(b) Electroluminescence polarization as a function of field applied at $4° \pm 2°$ to [01$\bar{1}$] for samples A and B, respectively, at several current densities. Each curve is labeled by the current density in units of A/cm^2. (c) Sample A ELP (points) as a function of field, with a -2.15% offset removed, and model ELP signal (solid curve) scaled by a factor of 20. (d),(e) Model ELP signal, including the effective nuclear field, as a function of applied field for samples A and B, respectively. The curves are labeled by the effective field b_N in kG [see Eq. (2)]. (f) Hanle curves measured for samples A and B. Curves in (a), (b), (d), and (e) are offset for clarity.

Under the assumption that the magnetization reversal in the ferromagnet occurs by coherent rotation [16], the angle between $\mathbf{M}$ and $\mathbf{B}_a$, and hence the orientation of the injected spin $\mathbf{S}_0$ can be determined from the magnetization data. The spin dynamics in the semiconductor are modeled using the formalism developed for the optical Hanle effect [11]:

$$\frac{d\mathbf{S}}{dt} = \frac{\mathbf{S}_0}{\tau} - \frac{\mathbf{S}}{\tau_s} - \frac{\mathbf{S}}{\tau} + \mathbf{\Omega} \times \mathbf{S}, \tag{1}$$

where τ_s^{-1} is the spin relaxation rate, τ^{-1} is the recombination rate, and $\mathbf{\Omega} = g^* \mu_B \mathbf{B}/\hbar$ is the Larmor frequency, where μ_B is the Bohr magneton.

The steady-state spin $\mathbf{S}$ that is measured by ELP can be found from Eq. (1) by setting $d\mathbf{S}/dt = 0$. We are interested in an upper bound for $\mathbf{S}$ and hence assume that $\mathbf{S}_0 = \epsilon \hat{\mathbf{m}}$, where $\epsilon = 0.42$ is the spin polarization of Fe [17] and $\hat{\mathbf{m}}$ is a unit vector parallel to $\mathbf{M}$. The parameters in Eq. (1) are thus reduced to two: the ratio $\alpha = \tau_s/\tau$, and the characteristic field scale $B_{1/2} = \hbar/(\mu_B g^* T_s)$, where $T_s^{-1} = \tau_s^{-1} + \tau^{-1}$. We determine α and the half-width $B_{1/2}$ by fitting the results of Hanle effect measurements, in which electron spins are optically injected along $\hat{\mathbf{z}}$ using circularly polarized light tuned near the band edge of the QW barriers. The circular polarization of the PL as a function of the transverse magnetic field is shown for both samples in Fig. 2(f). Fits to the expected Lorentzian shape [11] are shown as the solid curves. The dramatic difference in the widths of the two Hanle curves is due primarily to the different electron g factors in the two quantum wells.

Once the magnetization of the ferromagnet and the Hanle curve are known for each sample, it is possible to model the ELP signal *without any* free parameters. The result for sample A is shown as the solid curve in Fig. 2(c) along with data obtained at a current density of 3.6 A/cm^2. (A field-independent offset has been removed from the experimental data.) The ELP signal vanishes at large $\mathbf{B}_a$ because the injected spin is parallel to the field, and the signal vanishes at zero field because there is no precession. At intermediate fields, the magnetization is between the easy and hard axes, and the nonzero angle between $\mathbf{S}_0$ and $\mathbf{B}_a$ results in an ELP signal.

In spite of the general qualitative agreement in Fig. 2(c), the magnitude of the signal determined from our model is *smaller* than the experimental result by a factor of 20, even though we have already assumed a spin injection efficiency of unity. More significantly, the model of Eq. (1) cannot replicate the change in the shape of the ELP loops observed for sample B without requiring either the spin lifetimes or g^* to increase by over an order of magnitude with increasing current.

The most probable explanation for the discrepancy between the simple dynamical model and the experiment is that the effective magnetic field in the semiconductor is larger than the applied field and depends on the current density. This hypothesis is motivated by the observation of large internal magnetic fields in optical pumping experiments due to dynamic nuclear polarization (DNP) by electron spins [18–20]. In our experiment, the spins are injected electrically, and the magnitude of the nuclear polarization is determined by the current density [12]. The total magnetic field for electron spins is then the sum of the applied field $\mathbf{B}_a$ and a nuclear field [19]

$$\mathbf{B}_N = b_N \frac{(\hat{\mathbf{s}} \cdot \mathbf{B}_a)\mathbf{B}_a}{B_a^2 + B_0^2}, \tag{2}$$

where $\hat{\mathbf{s}}$ is a unit vector parallel to the injected spin, B_0 is the nuclear dipolar field, and b_N is the maximum nuclear field. We set B_0 to 2 G, a typical value for GaAs [19], and allow b_N to vary with current density. The total field $\mathbf{B} = \mathbf{B}_a + \mathbf{B}_N$ is then used in Eq. (1) to determine $\mathbf{S}$ and the expected ELP signal. The results of modeling with a nuclear field, adjusting b_N as the only free parameter, are shown in Figs. 2(d) and 2(e). Agreement with the observed magnitudes is obtained using values of b_N between 0 and 9 kG, which are indicated next to each curve. These are comparable to the internal fields obtained by optical pumping and are well below the maximum possible internal field of 5.3 T [19,21].

Including the effects of DNP also accounts for the major differences between the ELP curves observed for samples A and B. Although the shape of the ELP loops is nearly independent of current density for sample A, the position of the maximum signal observed for sample B shifts toward zero field as the current density increases, and the jump observed at larger applied fields disappears. The same trend is observed in the theoretical curves. The difference in behavior reflects the fact that the magnetization reversal in the two samples is essentially the same, while the widths of the Hanle curves differ by a factor of 6. In the case of sample A, the total internal field is less than the half-width of the Hanle curve. In this case, the average spin precesses only a fraction of a cycle before recombination, and the shape of the ELP loop is determined only by the rotation of the magnetization in the ferromagnet. In contrast, the maximum nuclear field in sample B exceeds the half-width of the Hanle curve, and hence spin precession in the semiconductor changes the shape of the ELP signal.

Although the data in Fig. 2 were obtained with a steady-state current flowing in the device, it is also possible to measure the ELP signal as a function of time after the current is turned on. In the case of sample B, we observe that the ELP signal increases to its steady-state value with a characteristic time of 10–50 sec, with full saturation reached in ≈ 5 min. This saturation process reflects the long nuclear spin relaxation time and is a distinguishing feature of DNP in semiconductors [18].

Given that only one parameter was varied to obtain the theoretical curves shown in Fig. 2, the overall agreement with the experiment provides strong support for

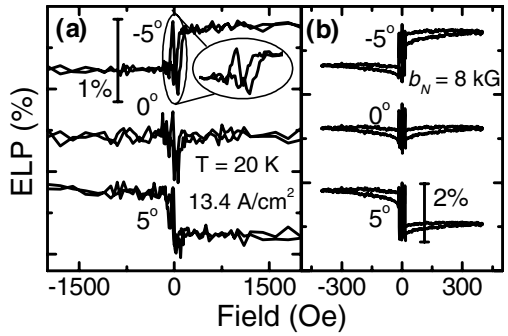

FIG. 3. (a) Sample B electroluminescence polarization data as a function of magnetic field for directions close to the [011] axis. The field is applied in the (100) plane (middle), and $\pm 5°$ out of the (100) plane (top and bottom curves). There is an in-plane rotation of 5° in all three cases. The inset shows an expansion of the region near zero field. (b) Modeling results for the sample orientations used in (a) in the presence of a nuclear field $b_N = 8$ kG.

DNP by electrical spin injection. The most important discrepancy between the data and the model occurs near zero field, where the suppression of the experimental signal occurs over a much wider field range than in the model. The narrow region observed in the model is based on the nuclear dipole field of 2 G for bulk GaAs. However, the suppression of DNP over a much wider field range has been observed in optical pumping studies of ferromagnet-semiconductor interfaces [7] and quantum dots [22].

Additional evidence for the existence of a nuclear field comes from data obtained for fields applied near the [011] axis. For fields parallel to [011], the magnetization of the Fe film is either parallel or antiparallel to $\mathbf{B}_a$ for any field, and the torque term in Eq. (1) is zero. As a result, no precession is expected. This is consistent with the behavior observed in the middle curve of Fig. 3(a), which was obtained for $\mathbf{B}_a$ in the (100) plane at an angle of 5° with respect to [011]. The top and bottom curves in Fig. 3(a) were obtained for rotations of the field axis $\pm 5°$ out of the (100) plane. Modeling of the ELP signal in this geometry, shown in Fig. 3(b), produces the steps observed in the data of Fig. 3(a) *only* if a nuclear field is included. The large nuclear polarization for applied fields near the easy axis is due to the dot product $\mathbf{S} \cdot \mathbf{B}_a$ in Eq. (2), which compensates for the fact that the torque term in Eq. (1) nearly vanishes. The dip in the signal at zero field shown in the inset of Fig. 3(a) is due to dipolar relaxation.

The efficiency of the DNP process should decrease with increasing temperature [23]. A strong suppression of the ELP signal with increasing temperature is seen in both samples, and no transverse ELP signal can be observed above 90 K. The evolution of the ELP signal with increasing temperature mirrors the changes seen in Fig. 2 as the current density decreases.

The approach to spin injection outlined in this Letter realizes the possibility of using conventional ferromagnets, small magnetic fields, and dc electrical currents to create and manipulate spin-polarized carriers in a semiconductor device. There remain several open questions, including a microscopic description of the DNP mechanism and its relation to the injection process. The connection with other approaches to DNP, such as "ferromagnetic imprinting" in optically pumped FM-S structures under *forward* bias [8,24], remains to be explored. Finally, a more detailed study of the transport properties of these FM-S systems will be required in order to achieve a purely electronic means of spin detection.

We acknowledge L. J. Sham and C. Ciuti for helpful discussions. This work was supported by ONR, the DARPA/ONR SPINS program, the University of Minnesota MRSEC (NSF DMR-0212032), and the Institute for Rock Magnetism. A. F. I. and B. D. S. thank 3M for support.

*Electronic address: crowell@physics.umn.edu

[1] S. Datta and B. Das, Appl. Phys. Lett. **56**, 665 (1990).
[2] P. R. Hammar and M. Johnson, Phys. Rev. Lett. **88**, 066806 (2002).
[3] H. J. Zhu *et al.*, Phys. Rev. Lett. **87**, 016601 (2001).
[4] A. T. Hanbicki *et al.*, Appl. Phys. Lett. **80**, 1240 (2002).
[5] V. F. Motsnyi *et al.*, Appl. Phys. Lett. **81**, 265 (2002).
[6] Y. Ohno *et al.*, Nature (London) **402**, 790 (1999).
[7] R. K. Kawakami *et al.*, Science **294**, 131 (2001).
[8] R. J. Epstein *et al.*, Phys. Rev. B **65**, 121202 (2002); R. J. Epstein *et al.*, cond-mat/0304030 [Phys. Rev. B (to be published)].
[9] R. Fiederling *et al.*, Nature (London) **402**, 787 (1999).
[10] A. W. Overhauser, Phys. Rev. **92**, 411 (1953).
[11] *Optical Orientation*, edited by F. Meier and B. P. Zakharchenya (North-Holland Physics Publishers, New York, 1984).
[12] M. Johnson, Appl. Phys. Lett. **77**, 1680 (2000).
[13] J. H. Smet *et al.*, Nature (London) **415**, 281 (2002).
[14] S. E. Barrett, R. Tycko, L. N. Pfeiffer, and K. W. West, Phys. Rev. Lett. **72**, 1368 (1994).
[15] D. J. Chadi, A. H. Clark, and R. D. Burnham, Phys. Rev. B **13**, 4466 (1976).
[16] E. C. Stoner and E. P. Wohlfarth, Philos. Trans. R. Soc. London, Ser. A **240**, 599 (1948).
[17] R. Meservey and P. M. Tedrow, Phys. Rep. **238**, 173 (1994).
[18] G. Lampel, Phys. Rev. Lett. **20**, 491 (1968).
[19] D. Paget, G. Lampel, B. Sapoval, and V. I. Safarov, Phys. Rev. B **15**, 5780 (1977).
[20] G. P. Flinn *et al.*, Semicond. Sci. Technol. **5**, 533 (1990).
[21] G. Salis, D. D. Awschalom, Y. Ohno, and H. Ohno, Phys. Rev. B **64**, 195304 (2001).
[22] D. Gammon *et al.*, Phys. Rev. Lett. **86**, 5176 (2001).
[23] A. Abragam, *Principles of Nuclear Magnetism* (Oxford University Press, Oxford, 1961).
[24] C. Ciuti, J. P. McGuire, and L. J. Sham, Phys. Rev. Lett. **89**, 156601 (2002).